L-subshell ionization of heavy elements by carbon and nitrogen ions of energy 0.4–1.8 MeV/amu

J. Semaniak, J. Braziewicz, and M. Pajek
Institute of Physics, Pedagogical University, 25-509 Kielce, Poland

T. Czyżewski, L. Głowacka, and M. Jaskóła
Soltan Institute for Nuclear Studies, 05-400 Otwock-Swierk, Poland

M. Haller, R. Karschnick, and W. Kretschmer
Physikalisches Institut, Universität Erlangen-Nürnberg, D-91058 Erlangen, Germany

Z. Halabuka and D. Trautmann
Institute of Physics, University of Basel, CH-4056 Basel, Switzerland
(Received 4 August 1994)

L-shell x-ray production and subshell ionization cross sections have been measured for 0.4–1.8-MeV/amu carbon and nitrogen ions for selected heavy elements with $72 \leq Z_2 \leq 90$. The results are compared with the predictions of the ECPSSR theory [perturbed-stationary-state (PSS) theory with energy-loss (E), Coulomb deflection (C), and relativistic (R) corrections] describing both direct ionization and electron-capture processes and the semiclassical approximation (SCA) calculations for direct ionization. For both theories significant deviations are found for L_2-subshell ionization in the low-energy range. The multiple ionization of outer shells was studied by comparing L x-ray intensity ratios measured for heavy ions and protons. The ionization probabilities of the N_4 subshell at zero impact parameter was extracted from these data. Measured ionization probabilities are compared with the predictions of the SCA theory and the "geometrical model." The influence of multiple ionization on the measured L-subshell cross sections is discussed.

PACS number(s): 34.50.−s

I. INTRODUCTION

A growing interest in inner-shell ionization by light ions, stimulated by both the development of x-ray analytical methods (e.g., the particle-induced x-ray emission) and the need for a deeper understanding of the fundamental process of the interaction of ions with matter, has resulted in many experimental and theoretical works in the past two decades. The experiments, concerning K-, L-, and M-shell ionization, were mostly limited to the light projectile such as protons and helium ions [1–7]. Simultaneously with experimental studies, both classical and quantum-mechanical models were developed for describing direct ionization, which is the dominating mechanism of vacancy production in asymmetric collisions ($Z_1 \ll Z_2$), where Z_1 and Z_2 are the projectile and target atomic numbers, respectively. Generally, the direct ionization can be described within the plane-wave Born approximation (PWBA) [8] and the semiclassical approximation (SCA) [9]. Both approaches were further improved to include the hyperbolic trajectories for the incident projectiles [10–12], the use of relativistic wave functions [13–17] and the correction for the "binding-polarization effect" [18–20]. The most advanced theory based on PWBA, including the corrections listed above, is known as the perturbed-stationary-state (PSS) theory with energy-loss, Coulomb deflection, and relativistic corrections (ECPSSR) of Brandt and Lapicki [21]. State-of-the-art calculations based on the SCA model have been described by Trautmann and coworkers [22,23].

Theoretical models give a good description of the K-shell ionization in a broad range of projectile energies and target atomic numbers for protons and helium ions. The same is also true for L-shell ionization by protons. However, for heavier projectiles, the experimental data are not in agreement with the first-order ionization theories, particularly for the case of L-subshell ionization processes in the low-energy range. Serious discrepancies between experimental data and theoretical predictions were already found for helium ions [24,25]. The principal reason for such discrepancies is the fact that the theoretical approaches mentioned above are treating L subshells independently, neglecting the coupling effects. The possible vacancy transfer between subshells during the collision modifies the L-subshell ionization cross sections [26–28]. The binding and polarization effects, which cannot be described properly in first-order calculations, are also expected to contribute to the observed discrepancies for heavier ions, due to stronger perturbation of the initial electronic wave function. In order to quantify these effects more systematically, more experimental data concerning L-subshell ionization by heavy ions are needed, especially in the low-energy regime. The number of experimental studies concerning L-shell ionization by projectiles heavier than protons and helium ions is rather limited. For instance, for carbon and nitrogen ions, which are a subject of the present work, we have found only a few publications. For carbon ions, Sarkadi and Mukoyama [29] reported L_i-subshell ionization cross sec-

tions for gold in the energy range 0.4–3.4 MeV, Malhi and Gray [30] measured individual L x-ray cross sections for Yb and Au at energies of 6–36 MeV, and Mehta *et al.* [31] reported total L x-ray production cross sections for different elements from Cu to Pb in the energy range 2.0–25.0 MeV. For nitrogen ions the situation is similar. The most often studied element is Au, which was investigated by Sarkadi and Mukoyama [29] in the ion energy range 1.7–2.8 MeV and by Pálinkás *et al.* [32] for ion energies of 3.0–18.2 MeV. The individual L x-ray production cross sections for Au and Yb targets bombarded by 7.0–42.0-MeV nitrogen ions were reported by Malhi and Gray [30]. Bauer *et al.* [33] have measured total L-shell x-ray production cross sections for Ag, Ta, and Au targets for nitrogen ion energies 0.125–4.0 MeV/amu.

In the present work, we study L-subshell ionization of some heavy elements between Hf and Th by $^{12}C^{3+}$ and $^{14}N^{3+}$ ions in the energy range 0.4–1.8 MeV/amu. The investigations cover the range of atomic number ratios $0.067 < Z_1/Z_2 < 0.097$ and the reduced velocities $0.095 < v_1/v_2 < 0.250$, where v_1 and v_2 denote the projectile and target electron velocities, respectively. The possible influence of multiple ionization on the change of the atomic parameters, used for calculation of L-subshell ionization cross sections, is discussed.

The measured cross sections are compared with those predicted by the ECPSSR theory, which describes both direct-ionization (DI) and electron-capture (EC) processes. We also make a comparison with the SCA calculations of Trautmann and Kauer [23] but only for the DI process. This is justified by the fact that for low charge states of carbon and nitrogen ions ($q = 3+$) the EC process contributes less than 5% to the total ionization cross section, as was estimated using the ECPSSR theory.

II. EXPERIMENTAL AND DATA ANALYSIS PROCEDURE

A. L-subshell ionization cross sections

Ion beams of $^{12}C^{3+}$ and $^{14}N^{3+}$ were obtained from the Tandem accelerator at the Institute of Physics of the University of Erlangen-Nürnberg. The measurements were performed at incident energies ranging from 0.4 to 1.8 MeV/amu. Prior to entering the target chamber, the beam was collimated to a diameter of 2 mm. Thin targets (4–50 μg/cm^2) of Hf, Ta, W, Os, Ir, Pt, Au, Bi, and Th were irradiated with typical beam currents of about 10–20 nA, which were monitored by the charge collection on target and Faraday cups. The targets were prepared by evaporating the elements in vacuum onto 10–20-μg/cm^2 carbon backing foils. The targets were mounted at an angle of 30° with respect to the beam direction. X rays were detected by an ultralow-energy Canberra HP Ge detector having a resolution of 150 eV at 6.4 keV. The detector was placed outside the target chamber, perpendicular to the beam axis. The x rays, before reaching the active volume of the detector, passed through a 25-μm metallized Mylar chamber window, a 10-mm air gap, and a 25-μm beryllium detector window. A Mylar filter (10 or 15 μg/cm^2) was applied occasionally to attenuate strong M-shell x rays. The x-ray detector efficiency was carefully calibrated in two ways. For energies above about 12 keV, calibrated ($\pm 3\%$) x- and γ-ray sources of ^{133}Ba, ^{152}Eu, and ^{241}Am were used. The efficiencies between 2 and 28 keV were obtained from measurements of K x-ray yields for a set of thin calibrating targets (from S to Sn) bombarded by 3-MeV protons. The "reference" K-shell ionization cross sections of Paul and Muhr [4] were used for this purpose. Special care was devoted to making an accurate determination of the detector efficiency close to the Ge K absorption edge, where L x-rays of the elements under study occur. A procedure suggested originally for Si (Li) detectors by Pajek *et al.* [34] has been extended to HPGe detectors and used to analyze the detector efficiency in our case. We found that the observed increase of the detector efficiency above the Ge-K absorption edge (see Fig. 1) could not be explained by the detector model used [34]. In this situation the fitting was performed independently in two energy regions, namely, below and above the Ge-K absorption edge, resulting in overall efficiency uncertainties of about 4%. We also note here that a similar efficiency curve for the Canberra HPGe detector was reported by other authors [35]. This indicates that the explanation of the observed increase of efficiency for a higher plateau needs further study.

Measured L x-ray spectra were analyzed using a nonlinear least-squares code ACTIV [36]. Individual Ll, $L\alpha_{1,2}$, $L\eta$, $L\beta_{4,6}$, $L\beta_1$, $L\beta_{2,3}$, $L\beta_{5,7,9}$, $L\gamma_5$, $L\gamma_1$, $L\gamma_{2,3,6,8}$, and $L\gamma_{4,4'}$ x-ray lines were fitted using Gaussian peaks on a polynomial background. Because $L\gamma_1$ and $L\gamma_{2,3,6,8}$ lines were further used to extract L_1- and L_2-subshell ionization cross sections, special care was devoted to the analysis of L lines, which were not fully resolved by the x-ray detector. Namely, we used single Gaussians for fitting $L\gamma_5$, $L\gamma_1$, and $L\gamma_{4,4'}$ peaks, while two Gaussians were necessary to fit the $L\gamma_{2,3,6,8}$ line, especially for heavier targets. This is partly connected with the natural structure of the analyzed peak consisting of two pairs of lines, namely, $L\gamma_2$, $L\gamma_3$, and $L\gamma_6$, $L\gamma_8$, being the transitions to L_1 and L_2 subshells, respectively. For example,

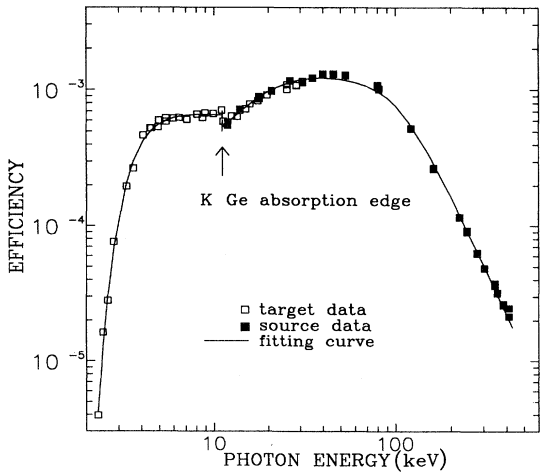

FIG. 1. X-ray detector (HPGe) efficiency curve.

for the Au target bombarded by 16.8-MeV nitrogen ions, the relative intensities of these lines, assuming 100% for the $L\gamma_1$ x-ray line, were estimated to be about $I(L\gamma_8)$:$I(L\gamma_2)$: $I(L\gamma_6)$:$I(L\gamma_3)$=0.8:8:9.4:10 [40]. The energy difference between the extreme $L\gamma_2$ and $L\gamma_3$ lines was of the order of 100 eV. Due to the additional broadening of $L\gamma$ lines caused by the outer-shell multiple ionization, it was not possible to resolve the structure of the $L\gamma_{2,3,6,8}$ peak uniquely. Consequently, for the determination of L_1-subshell ionization cross sections using the $L\gamma_{2,3,6,8}$ line, the complex nature of this line was taken into account [see Eq. (3a)]. A typical L x-ray spectrum, measured for an Au target bombarded by 14-MeV nitrogen ions, is shown in Fig. 2 together with the result of L x-rays fitting.

For determination of the L x-ray production cross sections, the individual x-ray yields were normalized to the number of projectiles scattered elastically into a Si surface barrier detector, placed at $\Theta=150°$ relative to the beam axis. Assuming that the x rays emitted from the targets have an isotropic distribution, the x-ray production cross sections $\sigma_x(E)$ were obtained from the data using the following expression:

$$\sigma_x(E)=\frac{N_x}{N_{\rm el}}\frac{\sigma_{\rm el}(\theta,E)\Omega_d}{\varepsilon(E_x)}F(E,\Delta E)\ , \tag{1}$$

where N_x and $N_{\rm el}$ are the numbers, corrected for dead time, of detected x rays and projectiles scattered elastically into the detector solid angle Ω_d, respectively, and $\varepsilon(E_x)$ is the x-ray detector efficiency. The screened elastic cross section $\sigma_{\rm el}(\theta,E)$ for heavy ions has been calculated following Huttel *et al.* [37]. The correction factor $F(E,\Delta E)$ included in our formula takes into account both x-ray absorption and the energy loss of ions in the target. Assuming that the x-ray production cross section $\sigma_x(E)$ and the stopping power $S(E)$ depend on the energy as E^α and E^β, respectively, we have obtained the following approximate expression for the correction factor:

$$F(E,\Delta E)=\left[1+\tfrac{1}{2}(2+\beta)-\tfrac{1}{6}(2+\beta)(3+\beta)\left[\frac{\Delta E}{E}\right]^2\right]\times\left\{1-\tfrac{1}{2}(\alpha-\beta+\mu\bar{x})\frac{\Delta E}{E}+\tfrac{1}{6}[(\alpha-\beta)(\alpha-\beta-1)(2\alpha-3\beta)\mu\bar{x}+(\mu\bar{x})^2]\left[\frac{\Delta E}{E}\right]^2\right\}^{-1}\ , \tag{2}$$

where $\bar{x}=E\cos\gamma\cos\delta/S(E)$.

Here, γ and δ are the angles between the normal to the target and, respectively, the ion beam axis and the direction of the x-ray detector. An iterative procedure [38] was applied to extract α from the measured x-ray production cross sections. Practically, three iterations were sufficient to determine α with an accuracy of less than 1%. The values of β were calculated using the heavy-ion stopping powers of Ziegler, Biersack, and Littmark [39]. We have checked that the correction procedure described above is accurate within 5% when the relative energy loss of ions is less than 25%. For the thickest target investigated, namely, 48 μg/cm^2 Ta, the estimated energy loss was about 230 keV for 5.6-MeV nitrogen ions. In this case, the cross-section correction was about 11%.

The measured $L\alpha_{1,2}$, $L\gamma_1$, and $L\gamma_{2,3,6,8}$ x-ray production cross sections were converted to the L-subshell ionization cross sections using the following expressions.

$$\sigma_{L_1}=\left[\sigma_{\gamma_{2,3,6,8}}-\sigma_{\gamma_1}\frac{\Gamma_{\gamma_{6,8}}}{\Gamma_{\gamma_1}}\right]\frac{\Gamma_1}{\Gamma_{\gamma_{2,3}}}\frac{1}{\omega_1}\ , \tag{3a}$$

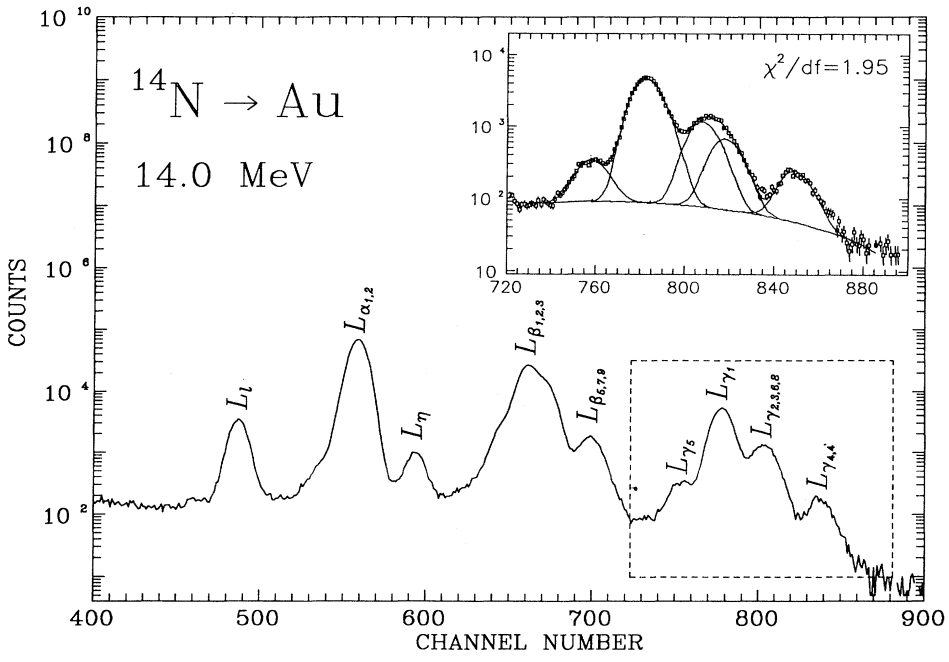

FIG. 2. L x-ray spectrum of an Au target bombarded by 14.0-MeV nitrogen ions. The result of the L x-ray group fitting is shown with the corresponding χ^2 per degree of freedom (df).

$$\sigma_{L_2}=\frac{\sigma_{\gamma_1}}{\omega_2}\frac{\Gamma_2}{\Gamma_{\gamma_1}}-f_{12}\sigma_{L_1}\ , \tag{3b}$$

$$\sigma_{L_3}=\frac{\sigma_{\alpha_{1,2}}}{\omega_3}\frac{\Gamma_3}{\Gamma_{\alpha_{1,2}}}-(f_{13}+f_{12}f_{23})\sigma_{L_1}-f_{23}\sigma_{L_2}\ , \tag{3c}$$

where the total (Γ_i) and individual ($\Gamma_{\alpha_i,\gamma_i}$) radiative rates were taken from Scofield [40]. For fluorescence, ω_i and Coster-Kronig transition yields f_{ij} the values from Chen, Crasemann, and Mark [41] were adopted.

Final uncertainties of the measured ionization cross sections were estimated as 6–20 % for the L_1 subshell, 5–12 % for the L_2 subshell, and 4–10 % for the L_3 subshell. They were caused, mainly, by the 3–4 % uncertainty of efficiency calibration of the HPGe detector and statistical uncertainties of x-ray yields, especially for the weakest $L\gamma_{2,3,6,8}$ line ($<3\%$), used in the derivation of L-shell ionization cross sections. An exception was the thinnest Th target (3.5 μg/cm^2), where this uncertainty was up to 6%. The accuracy of the ion-beam energy is of the order of 0.1%. This introduces an additional systematic uncertainty of the measured cross sections of less than 1% for the lowest energies studied.

B. Multiple ionization effects

All atomic parameters, used for obtaining the L-subshell ionization cross sections, were calculated for a single-vacancy configuration. However, for heavy ions the probability of producing more than one vacancy during a collision cannot be neglected. The effect of multiple ionization is usually studied by analyzing the satellite x-ray line structure measured with a high-resolution x-ray spectrometer. To extract the information about multiple vacancies from measurements with lower-resolution detection, we use a method proposed by Berinde *et al.* [42]. This method is based on the fact that relative intensities of lines filling a vacancy in the same subshell are influenced by the presence of additional vacancies in the levels from where the lines originate. Thus these relative intensities can give information about multiple ionization including vacancies in the higher subshells. This happens, for instance, when the probabilities of ionizing the corresponding initial states differ substantially from each other. For L-shell ionization, to study the effect of simultaneous multiple ionization of the M and N shells, the appropriate x-ray intensity ratios are $I(Ll(L_3-M_1))/I(L\alpha_{1,2}(L_3-M_{4,5}))$ and $I(L\eta(L_2\text{-}M_1))/I(L\gamma_1(L_2-N_4))$, respectively. To extract the M- and N-shell ionization probabilities, these ratios have to be measured under the same conditions both for heavy ions and, for instance, protons, for which the multiple ionization effect is not expected to play a role. Consequently, by comparing $I(Ll)/I(L_{1,2})$ and $I(L\eta)/I(L\gamma_1)$ ratios and assuming $p_{M_1}\ll p_{M_{4,5}}$, the authors of Ref. [42] obtained the following formulas for ionization probability per electron for $M_{4,5}$ and N_4 subshells, simultaneously with L-shell ionization:

$$(I_l/I_{\alpha_{1,2}})_{\rm HI}=(1-p_{M_{4,5}})^{-1}(I_l/I_{\alpha_{1,2}})_p\ , \tag{4a}$$

$$(I_\eta/I_{\gamma_1})_{\rm HI}=(1-p_{N_4})^{-1}(I_\eta/I_{\gamma_1})_p\ , \tag{4b}$$

where the subscripts HI and p stand for heavy ions and protons, respectively. We point out, however, that the assumption $p_{M_1}\ll p_{M_{4,5}}$ is not strictly valid. For instance, the M-subshell ionization probabilities are comparable when calculated with the SCA theory for an ion energy $E\approx 2$ MeV/amu. Consequently, by including both the ionization probability for the M_1 subshell and the alignment in (4a) and (4b), the following formulas are obtained:

$$(I_l/I_{\alpha_{1,2}})_{\rm HI}=\frac{1-p_{M_1}}{1-p_{M_{4,5}}}\frac{1-0.225kA_{20}^{\rm HI}(E)}{1-0.225kA_{20}^{p}(E)}(I_l/I_{\alpha_{1,2}})_p\ , \tag{5a}$$

$$(I_\eta/I_{\gamma_1})_{\rm HI}=\frac{1-p_{M_1}}{1-p_{N_4}}(I_\eta/I_{\gamma_1})_p\ , \tag{5b}$$

where $A_{20}^{{\rm HI},p}(E)$ is the alignment parameter for heavy ions and protons, respectively, and k corrects for the transfer of vacancies from the L_1 and L_2 subshells to the L_3 subshell [43]. From the SCA calculations we found that $p_{M_1}\approx 0.01$ and $p_{N_4}\approx 0.10$, thus justifying Eq. (4b). This means that using Eq. (5b), the value of p_{N_4} can easily be obtained. Moreover, combining Eqs. (5a) and (5b), one finds

$$\frac{(I_l/I_{\alpha_{1,2}})_{\rm HI}}{(I_\eta/I_{\gamma_1})_{\rm HI}}=\frac{1-p_{N_4}}{1-p_{M_{4,5}}}\frac{1-0.225kA_{20}^{\rm HI}(E)(I_l/I_{\gamma_1})_p}{1-0.225kA_{20}^{p}(E)(I_\eta/I_{\alpha_{1,2}})_p}\ , \tag{6}$$

from which $p_{M_{4,5}}$ can be estimated when p_{N_4} is known. In this way, both $p_{M_{4,5}}$ and p_{N_4} can generally be derived from the measurements. For the proton energies studied, the intensity ratios are expected to be defined by the ratios of corresponding radiative widths, namely, $I_l/I_{\alpha_{1,2}}\approx\Gamma_l/\Gamma_{\alpha_{1,2}}$ and $I_\eta/I_{\gamma_1}\approx\Gamma_\eta/\Gamma_{\gamma_1}$, which is due to neglecting the multiple ionization and the alignment in this case.

In order to measure the simultaneous L-shell and $M_{4,5}$- or N_4-subshell ionization probabilities, additional measurements were performed using thicker Au (250-μg/cm^2) and Bi (200-μg/cm) targets, to assure better statistics for weak L lines. The measurements were performed using both C and N ions and 3-MeV protons. Low-energy M x-rays, induced in the targets, were attenuated by a 200-μm Mylar absorber to keep dead-time correction below 8%. We have found that for proton excitation the intensity ratios for $L\eta$ and $L\gamma_1$ x-ray transitions agree with Scofield's radiative widths [40] within 12% for Au and 5% for Bi. For the ratios of Ll and $L\alpha_{1,2}$ transitions, the agreement is within 3%.

III. RESULTS AND DISCUSSION

A. L-subshell ionization cross sections

The experimental L_i-subshell ionization cross sections for C and N ions for the investigated targets are summa-

rized in Tables I and II, respectively, where the average total experimental uncertainties are also listed.

For L-subshell ionization of atoms with $72 \leq Z_2 \leq 90$ by carbon and nitrogen ions, we found only the cross sections for gold reported by other authors [29,30,32]. These data are compared with our results and with the predictions of SCA and ECPSSR theories in Figs. 3 and 4. For carbon ions, the cross sections for L_2 and L_3 subshells measured by Malhi and Gray [30] are about 30% smaller than ours. For the L_1 subshell our results are higher by up to 80%. Present results for N ions, shown in Fig. 4, are in good agreement with the data of Pálinkás *et al.* [32] and recent data of Malhi and Gray [30].

The measured L-subshell ionization cross sections are compared with the predictions of the ECPSSR and SCA theories. The ECPSSR theory, developed by Brandt and Lapicki [20,21], describes both the direct-ionization and the electron-capture processes within the PWBA and Oppenheimer-Brinkman-Kramers-Nikolaev approximation, respectively. These approximations were further corrected [20,21,44] in the ECPSSR theory for the following effects: the binding-polarization phenomena treated in a framework of the perturbed-stationary-state formalism; the Coulomb deflection (C) of the projectile; the relativistic (R) and, so-called, energy-loss (E) effects. For the initial charge state of carbon and nitrogen ions being $q = 3+$ in the present experiment, the ECPSSR theory predicts that the EC process contributes less than 4% to the ionization cross sections.

The SCA calculations used in the present work were

TABLE I. L-subshell ionization cross sections (in barns) measured for C ions and the average experimental uncertainties. The numbers in brackets represent factors of powers of 10.

Energy (MeV)	L_1	L_2	L_3	L_1	L_2	L_3	L_1	L_2	L_3
		Hf			Ta			W	
4.8	0.105 [+2]	0.229 [+2]	0.474 [+2]	0.556 [+1]	0.197 [+2]	0.402 [+2]	0.645 [+1]	0.150 [+2]	0.407 [+2]
6.0	0.208 [+2]	0.400 [+2]	0.911 [+2]	0.120 [+2]	0.382 [+2]	0.899 [+2]	0.971 [+1]	0.285 [+2]	0.781 [+2]
7.2	0.318 [+2]	0.764 [+2]	0.201 [+3]	0.186 [+2]	0.673 [+2]	0.163 [+3]	0.157 [+2]	0.480 [+2]	0.145 [+3]
9.6	0.727 [+2]	0.149 [+3]	0.423 [+3]	0.407 [+2]	0.128 [+3]	0.362 [+3]	0.283 [+2]	0.976 [+2]	0.333 [+3]
12.0	0.118 [+3]	0.222 [+3]	0.727 [+3]	0.684 [+2]	0.234 [+3]	0.650 [+3]	0.507 [+2]	0.165 [+3]	0.600 [+3]
14.4	0.148 [+3]	0.341 [+3]	0.106 [+4]	0.989 [+2]	0.388 [+3]	0.113 [+4]	0.787 [+2]	0.224 [+3]	0.692 [+3]
16.8	0.166 [+3]	0.383 [+3]	0.121 [+4]	0.149 [+3]	0.457 [+3]	0.143 [+4]	0.136 [+3]	0.373 [+3]	0.138 [+4]
19.2	0.378 [+3]	0.717 [+3]	0.226 [+4]	0.232 [+3]	0.612 [+3]	0.195 [+4]	0.170 [+3]	0.449 [+3]	0.155 [+4]
21.6	0.651 [+3]	0.832 [+3]	0.297 [+4]	0.355 [+3]	0.830 [+3]	0.265 [+4]	0.275 [+3]	0.598 [+3]	0.230 [+4]
Uncer. (%)	8–12	7–8	6–7	7–9	5–6	4–5	6–9	5–7	4–5
		Os			Ir			Pt	
4.8	0.546 [+1]	0.919 [+1]	0.232 [+2]	0.476 [+1]	0.878 [+1]	0.191 [+2]	0.545 [+1]	0.760 [+1]	0.140 [+2]
6.0	0.981 [+1]	0.199 [+2]	0.560 [+2]	0.919 [+1]	0.172 [+2]	0.472 [+2]	0.102 [+2]	0.140 [+2]	0.354 [+2]
7.2	0.157 [+2]	0.376 [+2]	0.106 [+3]	0.179 [+2]	0.317 [+2]	0.902 [+2]	0.140 [+2]	0.262 [+2]	0.713 [+2]
9.6	0.315 [+2]	0.762 [+2]	0.254 [+3]	0.296 [+2]	0.677 [+2]	0.219 [+3]	0.325 [+2]	0.580 [+2]	0.178 [+3]
12.0	0.512 [+2]	0.127 [+3]	0.463 [+3]	0.487 [+2]	0.112 [+3]	0.931 [+3]			
14.4	0.778 [+2]	0.194 [+3]	0.745 [+3]	0.599 [+2]	0.172 [+3]	0.619 [+3]	0.773 [+2]	0.147 [+3]	0.503 [+3]
16.8	0.114 [+3]	0.281 [+3]	0.106 [+4]	0.112 [+3]	0.242 [+3]	0.910 [+3]	0.989 [+2]	0.204 [+3]	0.746 [+3]
19.2	0.163 [+3]	0.362 [+3]	0.145 [+4]	0.135 [+3]	0.316 [+3]	0.123 [+4]	0.149 [+3]	0.266 [+3]	0.988 [+3]
21.6	0.290 [+3]	0.358 [+3]	0.211 [+4]	0.240 [+3]	0.410 [+3]	0.161 [+4]	0.260 [+3]	0.350 [+3]	0.130 [+4]
Uncer. (%)	10–17	8–11	5–7	8–17	5–7	4–5	8–10	5–7	4–5
		Au			Bi			Th	
4.8	0.537 [+1]	0.665 [+1]	0.111 [+2]	0.270 [+1]	0.325 [+1]	0.635 [+1]	0.355 [+0]	0.714 [+0]	0.191 [+1]
6.0	0.102 [+2]	0.135 [+2]	0.291 [+2]	0.507 [+1]	0.703 [+1]	0.165 [+2]	0.155 [+1]	0.158 [+1]	0.514 [+1]
7.2	0.163 [+2]	0.241 [+2]	0.600 [+2]	0.103 [+2]	0.134 [+2]	0.362 [+2]	0.168 [+1]	0.416 [+1]	0.122 [+2]
9.6	0.315 [+2]	0.476 [+2]	0.144 [+3]	0.196 [+2]	0.293 [+2]	0.941 [+2]	0.539 [+1]	0.105 [+2]	0.332 [+2]
12.0	0.587 [+2]	0.882 [+2]	0.270 [+3]	0.295 [+2]	0.423 [+2]	0.154 [+3]	0.132 [+2]	0.187 [+2]	0.629 [+2]
14.4	0.770 [+2]	0.149 [+3]	0.525 [+3]	0.378 [+2]	0.649 [+2]	0.244 [+3]	0.104 [+2]	0.270 [+2]	0.981 [+2]
16.8	0.124 [+3]	0.188 [+3]	0.630 [+3]	0.511 [+2]	0.105 [+3]	0.410 [+3]	0.220 [+2]	0.390 [+2]	0.150 [+3]
19.2	0.187 [+3]	0.269 [+3]	0.891 [+3]	0.560 [+2]	0.134 [+3]	0.581 [+3]	0.309 [+2]	0.547 [+2]	0.233 [+3]
21.6	0.252 [+3]	0.320 [+3]	0.116 [+4]	0.885 [+2]	0.191 [+3]	0.773 [+3]	0.301 [+2]	0.842 [+2]	0.359 [+3]
Uncer (%)	8–10	5–7	4–6	15–20	7–8	5–8	15–20	6–13	5–10

described by Trautmann and co-workers [22,23]. Briefly, this approach assumes that the motions of the projectile is along the classical hyperbolic trajectory, whereas the atomic electron is described quantum mechanically using the relativistic hydrogenlike wave functions. Here, the binding effect is simulated by the "united-atom" limit. Present SCA calculations predict only the direct ionization but, as was estimated above, a contribution due to electron capture is negligible.

In Figures 5 and 6, the measured L-subshell ionization cross sections for C and N ions, respectively, normalized to the ECPSSR predictions, are plotted against the scaled velocity $\xi_{L_i}=2v_1/v_{L_1}\theta_{L_i}$. Here v_1 and v_{L_i} are the projectile and electron velocities, respectively. The dimensionless parameter $\theta_{L_i}=n^2E_{L_i}/\mathcal{R}Z_{L_i}^2$ is the scaled L_i-subshell binding energy, where E_{L_i} is the observed electron binding energy, $\mathcal{R}$ is the Rydberg constant, n is the principal quantum number, and Z_{L_i} denotes the screened nuclear charge of the atom [45] in units of the electron charge.

The most striking discrepancy between theory and experiment is found for the L_2-subshell ionization by C and N ions (see Figs. 5 and 6), where the experimental data are strongly underestimated by the ECPSSR theory in the low-energy region. At the lowest velocities ($\xi\approx0.25$) the disagreement reaches a factor of about 10, and then

TABLE II. L-subhsell ionization cross sections (in barns) measured for N ions and the average experimental uncertainties. The numbers in brackets represent factors of powers of 10.

Energy (MeV)	L_1	L_2	L_3	L_1	L_2	L_3	L_1	L_2	L_3
		Hf			Ta			W	
5.6	0.875 [+1]	0.217 [+2]	0.398 [+2]	0.666 [+1]	0.186 [+2]	0.334 [+2]	0.500 [+1]	0.163 [+2]	0.303 [+2]
7.0	0.171 [+2]	0.452 [+2]	0.984 [+2]	0.141 [+2]	0.379 [+2]	0.825 [+2]	0.994 [+1]	0.323 [+2]	0.674 [+2]
8.4	0.265 [+2]	0.731 [+2]	0.170 [+3]	0.235 [+2]	0.643 [+2]	0.146 [+3]	0.176 [+2]	0.558 [+2]	0.126 [+3]
9.8				0.330 [+2]	0.851 [+2]	0.210 [+3]	0.215 [+2]	0.789 [+2]	0.200 [+3]
11.2	0.530 [+2]	0.135 [+3]	0.352 [+3]	0.459 [+2]	0.804 [+2]	0.208 [+3]	0.285 [+2]	0.106 [+3]	0.282 [+3]
12.6	0.797 [+2]	0.186 [+3]	0.489 [+3]	0.607 [+2]	0.141 [+3]	0.377 [+3]	0.462 [+2]	0.147 [+3]	0.389 [+3]
14.0	0.103 [+3]	0.222 [+3]	0.594 [+3]	0.796 [+2]	0.201 [+3]	0.517 [+3]	0.598 [+2]	0.203 [+3]	0.555 [+3]
16.8	0.180 [+3]	0.315 [+3]	0.839 [+3]	0.129 [+3]	0.279 [+3]	0.732 [+3]	0.968 [+2]	0.240 [+3]	0.604 [+3]
19.6				0.192 [+3]	0.382 [+3]	0.968 [+3]	0.134 [+3]	0.321 [+3]	0.832 [+3]
22.4	0.306 [+3]	0.544 [+3]	0.139 [+4]	0.265 [+3]	0.485 [+3]	0.118 [+4]	0.202 [+3]	0.422 [+3]	0.111 [+4]
Uncer. (%)	6–8	5–6	4–5	7–9	5–8	4–5	6–14	5–8	4–5
		Os			Ir			Pt	
5.6	0.491 [+1]	0.123 [+2]	0.208 [+2]	0.528 [+1]	0.108 [+2]	0.159 [+2]	0.560 [+1]	0.882 [+1]	0.126 [+2]
7.0	0.966 [+1]	0.250 [+2]	0.521 [+2]	0.104 [+2]	0.218 [+2]	0.417 [+2]	0.988 [+1]	0.177 [+2]	0.346 [+2]
8.4	0.197 [+2]	0.401 [+2]	0.933 [+2]	0.154 [+2]	0.359 [+2]	0.808 [+2]	0.177 [+2]	0.301 [+2]	0.691 [+2]
9.8	0.296 [+2]	0.608 [+2]	0.152 [+3]	0.204 [+2]	0.532 [+2]	0.132 [+3]	0.249 [+2]	0.443 [+2]	0.112 [+3]
11.2	0.407 [+2]	0.850 [+2]	0.226 [+3]	0.361 [+2]	0.731 [+2]	0.191 [+3]	0.344 [+2]	0.626 [+2]	0.166 [+3]
12.6	0.576 [+2]	0.112 [+3]	0.311 [+3]	0.437 [+2]	0.926 [+2]	0.256 [+3]	0.514 [+2]	0.783 [+2]	0.219 [+3]
14.0	0.723 [+2]	0.143 [+3]	0.422 [+3]	0.675 [+2]	0.132 [+3]	0.355 [+3]	0.719 [+2]	0.118 [+3]	0.320 [+3]
16.8	0.941 [+2]	0.191 [+3]	0.511 [+3]	0.656 [+2]	0.178 [+3]	0.484 [+3]	0.805 [+2]	0.154 [+3]	0.443 [+3]
19.6	0.141 [+3]	0.260 [+3]	0.703 [+3]	0.126 [+3]	0.227 [+3]	0.616 [+3]	0.129 [+3]	0.195 [+3]	0.532 [+3]
22.4	0.214 [+3]	0.311 [+3]	0.862 [+3]	0.199 [+3]	0.291 [+3]	0.718 [+3]			
Uncer. (%)	8–10	6–8	4–5	8–15	6–8	5–6	9–20	6–8	5–9
		Au			Bi			Th	
5.6	0.415 [+1]	0.905 [+1]	0.172 [+2]	0.234 [+1]	0.418 [+1]	0.572 [+1]	0.675 [+0]	0.105 [+1]	0.158 [+1]
7.0	0.106 [+2]	0.145 [+2]	0.262 [+2]	0.464 [+1]	0.844 [+1]	0.155 [+2]	0.815 [+0]	0.288 [+1]	0.504 [+1]
8.4	0.172 [+2]	0.247 [+2]	0.540 [+2]	0.747 [+1]	0.149 [+2]	0.334 [+2]	0.236 [+1]	0.558 [+1]	0.114 [+2]
9.8	0.252 [+2]	0.379 [+2]	0.936 [+2]	0.115 [+2]	0.216 [+2]	0.582 [+2]	0.521 [+1]	0.824 [+1]	0.223 [+2]
11.2	0.300 [+2]	0.517 [+2]	0.138 [+3]	0.167 [+2]	0.301 [+2]	0.843 [+2]	0.374 [+1]	0.127 [+2]	0.376 [+2]
12.6	0.474 [+2]	0.680 [+2]	0.189 [+3]	0.228 [+2]	0.444 [+2]	0.135 [+3]	0.648 [+1]	0.161 [+2]	0.564 [+2]
14.0	0.559 [+2]	0.910 [+2]	0.265 [+3]	0.309 [+2]	0.557 [+2]	0.173 [+3]	0.106 [+2]	0.222 [+2]	0.727 [+2]
16.8	0.760 [+2]	0.133 [+3]	0.375 [+3]	0.361 [+2]	0.763 [+2]	0.245 [+3]	0.117 [+2]	0.353 [+2]	0.124 [+3]
19.6	0.116 [+3]	0.179 [+3]	0.495 [+3]	0.483 [+2]	0.106 [+3]	0.333 [+3]	0.205 [+2]	0.500 [+2]	0.167 [+3]
Uncer. (%)	13–18	8–11	7–10	15–25	9–12	9–12	15–30	6–12	6–12

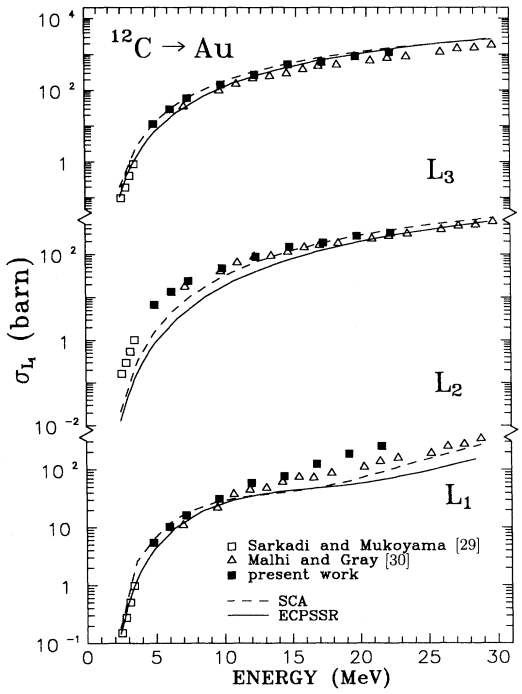

FIG. 3. L-subshell ionization cross sections of Au bombarded by carbon ions compared with the results of other authors and with predictions of the ECPSSR and SCA theories.

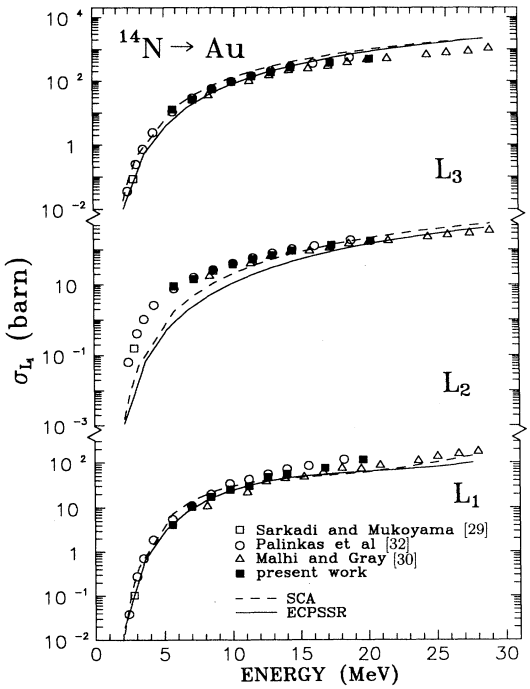

FIG. 4. L-subshell ionization cross sections of Au bombarded by nitrogen ions compared with the result of other authors and with predictions of the ECPSSR and SCA theories.

decreases gradually for higher velocities. Above $\xi \approx 0.55$ the theory describes the experimental data within experimental uncertainties. The same tendency is observed for the L_3 subshell, but here the discrepancies are not so strong. The low-energy data are, on average, by a factor of two higher than the theoretical predictions. For the L_3 subshell we found, however, that despite the good agreement between experiment and theory for C ions, substantial discrepancies by a factor of two are observed for N ions. L_1-subshell ionization cross sections agree within 40% with the ECPSSR theory for scaled velocities below 0.55. Above this value, the data are systematically higher than the theoretical predictions, up to a factor of 3. Similar general features are observed when comparing the present data with the SCA theory (see Figs. 7 and 8) despite an improved agreement for L_2 and L_3 subshells. Here, the discrepancies between experiment and theory for L_2 subshells are reduced to a factor of five for low energies. The SCA theory describes the measured L_3-subshell ionization cross sections better, but above $\xi \approx 0.5$ the data are systematically lower by about 20% for C ions, and reach a factor of two for N ions. For the L_1 subshell in the low-energy range, the present data are sys-

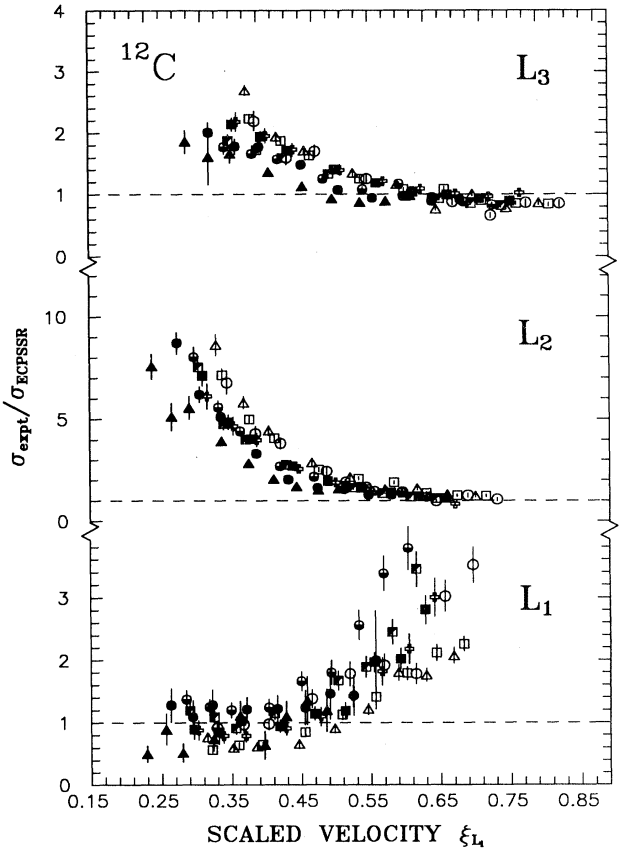

FIG. 5. Measured L-subshell ionization cross sections for carbon ions normalized to the ECPSSR-theory predictions, as a function of the scaled velocity ξ_{L_i}. Symbols used are the following: Hf, open circles; Ta, open squares; W, open triangles; Os, open crosses; Ir, full squares; Pt, black and white squares; Au, black and white circles; Bi, full squares; and Th, full triangles.

tematically 40% lower than the SCA predictions. As one can see in Figs. 5–8, the predictions of the SCA theory are in better agreement with the measured data in the low-energy regime. This arises from different approaches used to describe the binding effect in the two theories. In the SCA calculations this effect was simulated by the united-atom (UA) limit, which is generally justified in slow collisions ($\xi \ll 1$), for which the adiabatic distance is smaller than the orbital radius. For the present data, the scaled velocity assumes the values $0.2 < \xi < 0.8$, so the united-atom limit can be regarded only as an approximation to simplify the calculations. The binding correction used in the ECPSSR theory leads to an overestimation of the effective binding energy in the low-energy limit, exceeding even the UA value. This observation was pointed out by Vigilante *et al.* [46], who introduced the "saturation" of the binding correction into the ECPSSR theory, resulting in a significant improvement of the ECPSSR predictions for the L-shell ionization of medium-Z elements by helium ions [46]. Following this idea, we tried to explain the observed discrepancies at low energies by saturation of the binding energy at its UA value. We found, however, that contrary to the conclusion of Vigilante *et al.* [46], this modification does not appreciably change the cross sections for L-shell ionization for heavy elements by C and N ions. This surprising result is explained by a weaker dependence of the reduced binding energy θ on Z_2 for heavy elements, which does not change the UA binding energy with respect to its SA value as much as for the intermediate Z_2. To discuss this effect more quantitatively, the reduced electron binding energy, according to the prescription used in the ECPSSR theory for the united atom ($\xi = 0$), is compared with the experimental UA reduced binding energy for the $Z_{UA} = Z_1 + Z_2$ atom in Fig. 9 versus the projectile atomic number Z_1. Here one finds that for gold atoms the binding corrections used in the ECPSSR theory in the UA limit for L_1 and l_2 subshells agree very well with the experimental united-atom binding energies. For the L_3 subshell the ECPSSR binding correction overestimates the experimental binding energies by about 5% for C and N ions in the UA limit. However, since in the present experiment $\xi > 0.2$, this effect is expected to be even smaller due to a diminishing role of the binding effect for higher velocities.

The discussion above fully indicates the importance of a proper description of the binding effect in the low-energy regime. Further improvement of the calculations would be possible by performing a fully time-dependent

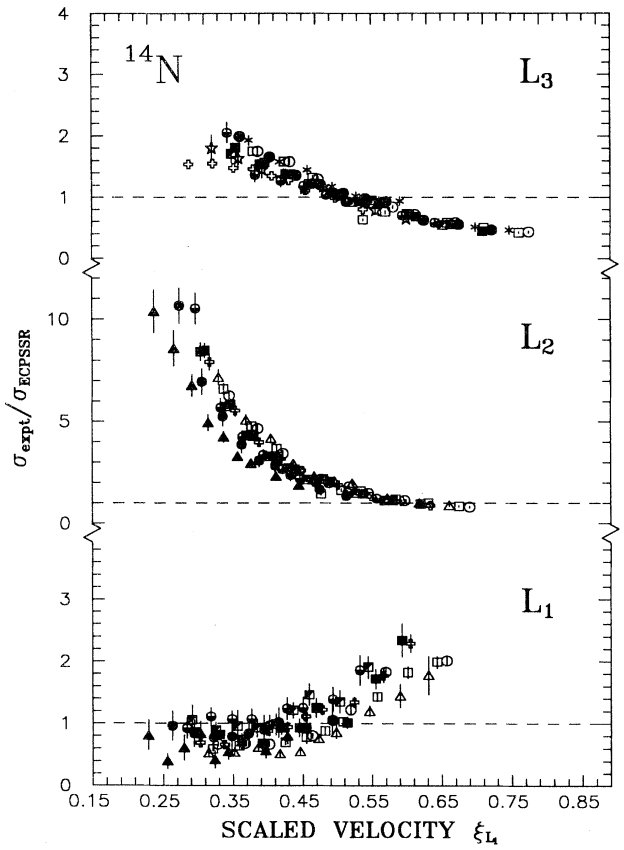

FIG. 6. Measured L-subshell ionization cross sections for nitrogen ions normalized to the ECPSSR-theory predictions, as a function of the scaled velocity ξ_{L_i}. The symbols used to mark different elements are the same as in Fig. 5.

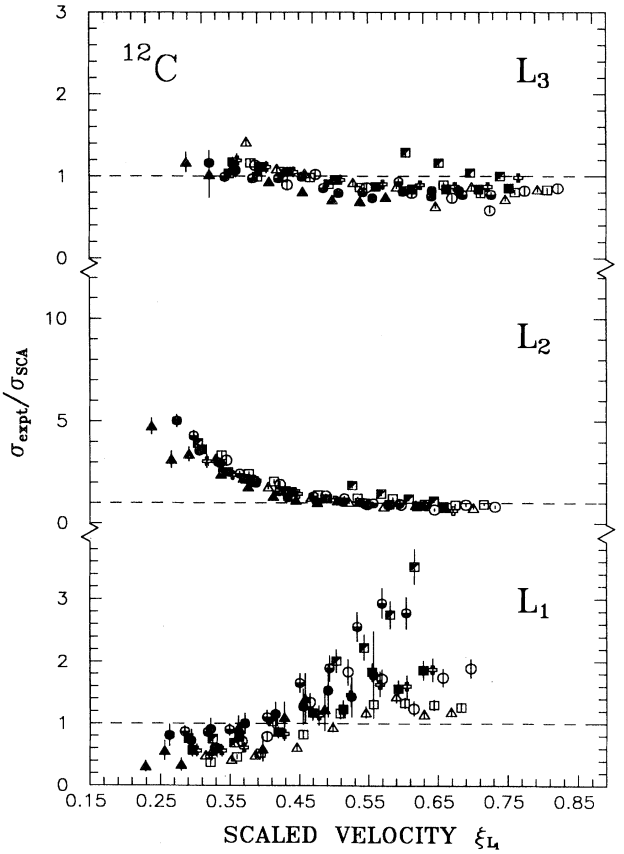

FIG. 7. Measured L-subshell ionization cross sections for carbon ions normalized to the SCA-theory predictions, as a function of the scaled velocity ξ_{L_i}. The symbols used to mark different elements are the same as in Fig. 5.

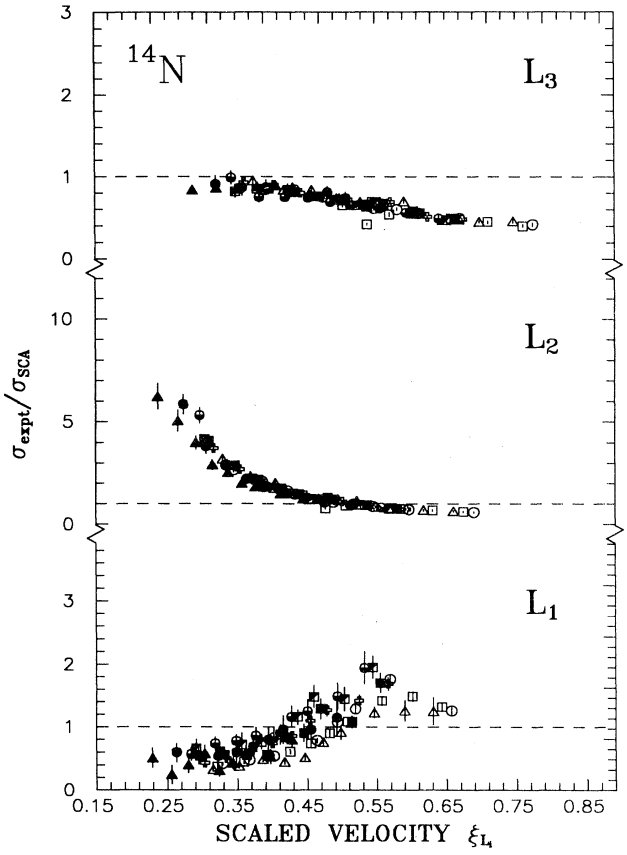

FIG. 8. Measured L-subshell ionization cross sections for nitrogen ions normalized to the SCA theory predictions, as a function of the scaled velocity ξ_{L_i}. The symbols used to mark different elements are the same as in Fig. 5.

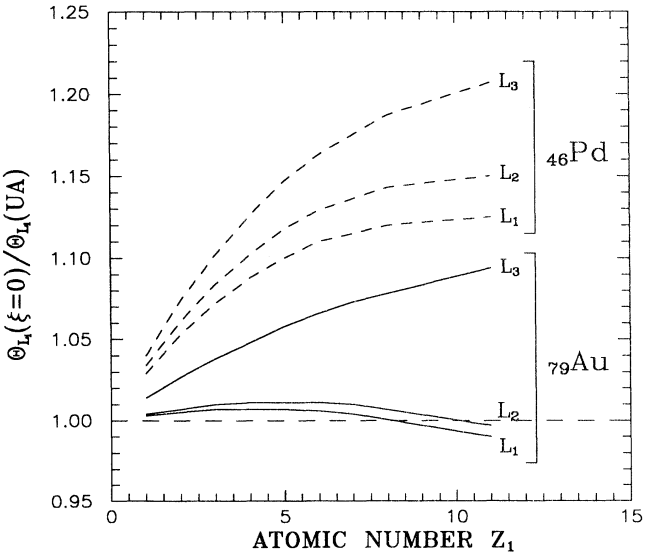

FIG. 9. Ratio of the reduced binding energy Θ_{L_i}, calculated according to the ECPSSR-theory formalism in the UA limit ($\xi=0$), to experimental UA binding energy.

binding correction in the SCA approach, as was done earlier for the K shell [47].

At higher ion energies ($\xi > 0.5$) the theoretical predictions overestimate the measured L_3-subshell ionization cross sections by about a factor of 2.5. A possible explanation for this disagreement can be found in the inadequate description of the binding-polarization effects in the medium velocity range ($\xi \sim 1$), where the polarization is expected to be strongest. It should be emphasized, however, that the polarization effect is not included in the SCA calculations. We also note here that the observed overestimation of present experimental results by the theoretical predictions is consistent with the data reported by other authors (see Fig. 4).

As was shown in Figs. 8 and 9, the SCA calculations performed in the UA limit cannot eliminate the strong underestimation of the experimental data by theory in the low-energy range. One possible explanation for this phenomenon is related to the couplings between L_i subshells. This effect was first studied by Sarkadi and Mukoyama [26] in a simple two-step model treating ionization and subshell couplings as two independent processes. This approximation was further refined by the same authors in a framework of a coupled-state model [27,48,49]. The performance of the coupled-state model for a description of L-subshell ionization of heavy elements induced by helium ions was tested by Sarkadi and Mukoyama [24]. They found that their model reduces the discrepancies between the experimental L_2-subshell ionization cross sections and the predictions of the first-order perturbation theory in the low-energy region by a factor of four. Also, Pálinkás *et al.* [32] showed that the two-step model successfully describes the measured L_i-subshell ionization cross sections for Au bombarded by nitrogen ions. The importance of coupling effects for L-shell ionization by ion impact has been studied in Refs. [50,51] by performing coupled-channel calculations.

The data for the L_1 subshell (Figs. 5–8) show, in general, a much bigger spread of experimental points compared to L_2 and L_3 subshells. The L_1-subshell ionization cross sections are derived from the weakest $L\gamma_{2,3,6,8}$ x-ray line, for which additionally a contribution of $L\gamma_{6,8}$ transition from the L_2 subshell has to be subtracted. Consequently, L_1-subshell ionization cross sections are more sensitive to the atomic parameters used for the conversion of the measured L x-ray cross sections into ionization cross sections. The fluorescence yields of Chen, Crasemann, and Mark [41] for the L_1 subshell are not in agreement with the data of Krause [52]. Additionally, both sets of ω_1 are for the single-vacancy configuration, and they can be further modified due to the multiple ionization of outer shells. This effect will be discussed in the next section.

B. Multiple ionization probabilities

The effect of multiple ionization of outer shells by heavy ions was studied by comparing the L x-ray spectra induced by protons with those measured for C and N ions adopting the method described in Sec. II B. Applying this method to $L\eta$ and $L\gamma_1$ x-ray lines, we determined,

using Eq. (6b), the probability per electron of simultaneous ionization of the L shell and the N_4 subshell. This was done by assuming that the ionization probability for the M_1 subshell is much smaller than the one for the N_4 subshell, i.e., $p_{M_1} \ll p_{N_4}$. Derived ionization probability versus reduced velocity v_1/v_2 is shown in Figs. 9 and 10 for C and N ions corresponding to Au and Bi targets, respectively. Present results are in good agreement with the data reported by Berinde *et al.* [42]. On the other hand, Bhattacharya *et al.* [53] reported data lying by a factor of three higher, which, due to a low x-ray energy resolution and poor statistics for the $L\eta$ line in their experiment were, in our opinion, overestimated.

The measured ionization probabilities can be compared with ionization probabilities at zero impact parameter, $p_{M_i}(0)$ and $p_{N_i}(0)$, because of the much smaller L-shell radius compared with the dimensions of M and N shells. Theoretical ionization probabilities $p_{M_i}(0)$ and $p_{N_i}(0)$ were calculated using the SCA theory and the "geometrical model" (GM) of Sulik *et al.* [54]. The geometrical model, based on the binary encounter approximation BEA [55], makes use of the scaling variable

$$x = 4\frac{Z_1}{v_1} V\sqrt{G(V)} ,$$

where $V = v_1/v_2$ is the reduced projectile velocity (v_2 denotes the atomic electron velocity) and $G(V)$ is the BEA scaling function. In calculations, we used the Gerjuoy-Vriens-Garcia $G(V)$ function tabulated by McGuire and Richard in Ref. [55]. The ionization probabilities were calculated using the geometrical model for two extreme cases, namely, for separated- and united-atom limits. The SCA calculations were performed in the UA limit using the relativistic hydrogenic wave functions. Figures 10 and 11 show that the predictions of the SCA theory for $p_{N_4}(0)$ agree with the measured data within the experimental uncertainties. On the other hand, the geometrical model predicts the ionization probability only within a factor of two. We have used SCA calculations to check the correctness of our assumption $p_{M_1}(0) \ll p_{N_4}(0)$, which was used to obtain the experimental values of ionization probabilities for the N_4 subshell. Indeed, we find that, according to the results of the SCA, $p_{M_1}(0) \approx 0.01$ and $p_{N_4}(0) \approx 0.10-0.18$ in the energy range 1–30 MeV. This implies that possible corrections due to neglecting $p_{M_1}(0)$ in Eq. (5b) are of the order of experimental uncertainties of ionization probabilities of about 30%.

The average ionization probabilities for the $M_{4,5}$ subshell, $p_{M_{4,5}}(0)$, can generally be derived from the measured $I(Ll)/I(L\alpha_{1,2})$ ratios, following the method described in Sec. II B [see Eq. (5b)]. Since the ionization probabilities for M_1 and $M_{4,5}$ subshells are, however, comparable, Eq. (5a) cannot be used in this case to extract $p_{M_{4,5}}(0)$ probabilities, as was the case for $p_{N_4}(0)$. For instance, the calculations of ionization probabilities performed within the SCA model showed that $p_{M_4}(0)$ and $p_{M_5}(0)$ probabilities are higher than $p_{M_1}(0)$ by about a factor of 2. Similar estimates were obtained by using the geometrical model. Moreover, the value of the $I(Ll)/I(L\alpha_{1,2})$ ratio also depends on the alignment parameter $A_{20}(E)$, which one is not well known for heavy ions. Since the absolute value of the ionization probability for $M_{4,5}$ subshells is about 0.02, which is comparable to the magnitude of the correction for alignment [see Eq. (6)], we have found that the ionization probability

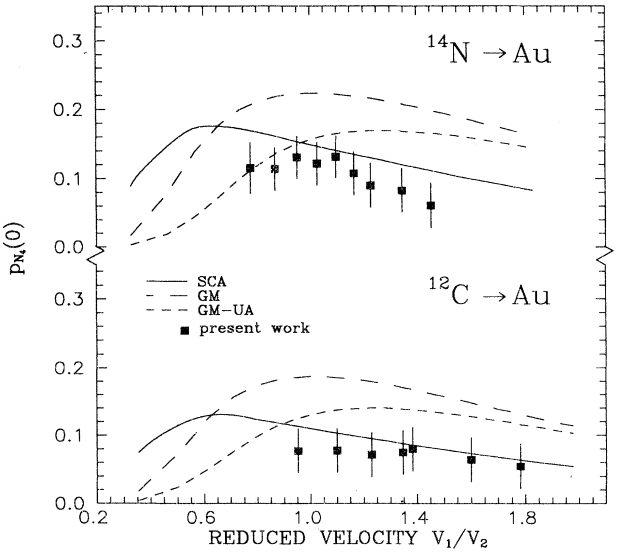

FIG. 10. N_4-subshell ionization probability per electron a zero impact parameter for Au bombarded by C and N ions vs the reduced velocity $V = v_1/v_2$. The experimental data are compared with the SCA calculations and the geometrical model predictions in separated-atom and united-atom limits.

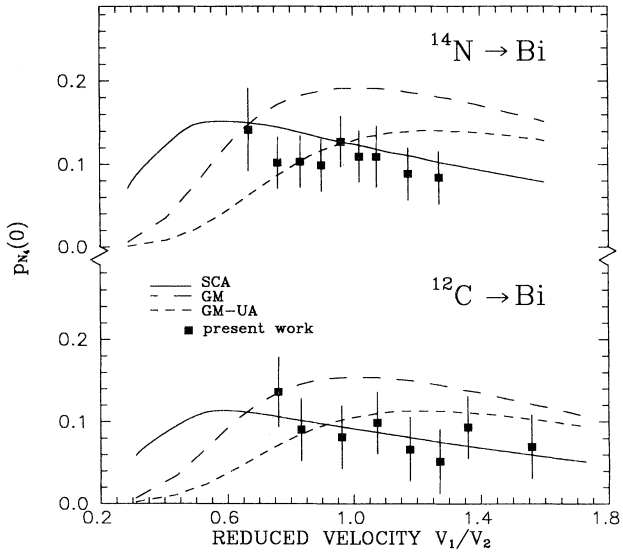

FIG. 11. N_4-subshell ionization probability per electron at zero impact parameter for Bi bombarded by C and N ions vs the reduced velocity $V = v_1/v_2$. The experimental data are compared with the SCA calculations and the geometrical model predictions in separated-atom and united-atom limits.

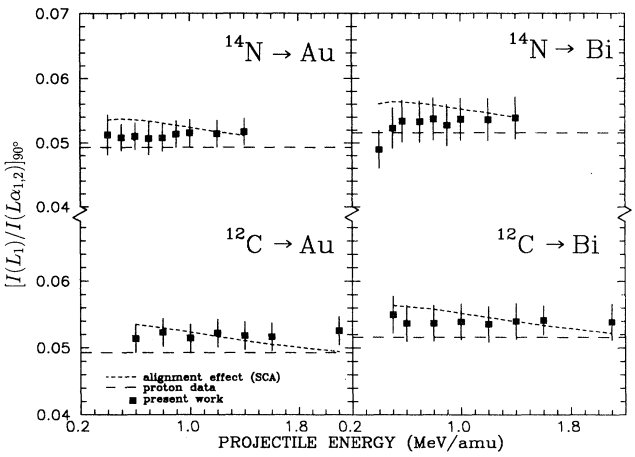

FIG. 12. $I(Ll)/I(L\alpha_{1,2})$ ratio measured at 90° relative to the beam axis (open squares) for Au and Bi targets bombarded by C and N ions. Theoretical predictions of the SCA L_3 alignment calculations are shown.

$p_{M_{4,5}}(0)$ cannot be derived with acceptable accuracy. Figure 12 shows that the measured $I(Ll)/I(L\alpha_{1,2})$ ratios are fairly well described by the SCA calculations. Some discrepancies observed at low energies were also reported by Jitschin *et al.* [56] and Pálinkás *et al.* [32], who succeeded in explaining them in terms of coupling effects [49].

The effect of multiple ionization of outer M and N shells causes the energy shift of L x-ray lines. This effect can thus be used to check independently the estimated ionization probabilities for M and N shells. Using the ionization probabilities $p_{M_i}(0)$ and $p_{N_i}(0)$ estimated from SCA calculations, we found that the expected x-ray energy shifts for L_1, $L\alpha_{1,2}$, $L\eta$, and $L\beta_1$ lines are below 20 eV. These energy shifts are, however, of the order of experimental uncertainties of x-ray energies, which are about 18 eV. Larger x-ray energy shifts were observed for $L\gamma$ x-ray lines. They were about 50 eV for $L\gamma_1$ and in the range of 100–150 eV for $L\gamma_{2,3,6,8}$ and $L\gamma_{4,4'}$ (see Table III). Using the SCA calculation, we determined the average x-ray energy shifts due to additional M- or N-shell vacancies for Au by taking the average energy shift per vacancy from Ref. [57]. In these estimates, the contribution of the vacancies in the O shell was neglected, because of the absence of data for this shell. The measured and calculated x-ray energy shifts for L lines are summarized in Table III. For the $L\gamma_1$ line the measured energy shifts agree with theoretical estimations. A discrepancy observed for $L\gamma_{2,3,6,8}$ can be explained by neglecting a contribution of the dominating L_1-O_1,O_4 transitions due to a lack of data for the O shell. For the same reason, we cannot estimate the theoretical energy shifts for the $L\gamma_{4,4'}$ line. We observe that the measured x-ray energy shifts scale with Z_i^2, as expected from first-order theories.

TABLE III. The average energy shifts of individual $L\gamma$ x-ray lines of Au and Bi bombarded by C and N ions due to the multiple ionization effect. Theoretical predictions estimated using SCA calculations are shown in parentheses.

	Au		Bi	
X line	$\Delta E(C)$	$\Delta E(N)$	$\Delta E(C)$	$\Delta E(N)$
$L\gamma_1$	39(48)	51(57)	48	68
$L\gamma_{2,3,6,8}$	95(45)	135(53)	113	152
$L\gamma_{4,4'}$	118	153	139	187

Using estimated ionization probabilities, we estimated a possible change of the atomic parameters for Au and Bi to be about 5% for relative individual radiative rates and 7% for the fluorescence yields. For this purpose, we made use of a simplified formula of Lapicki *et al.* [58], which assumes the same ionization probabilities per electron for all subshells that are outer with respect to a given shell. We have estimated this probability as a mean weighted value of the measured $p_{M_i}(0)$ and $p_{N_i}(0)$ probabilities. Finally, we found that the expected change of the atomic parameters due to multiple ionization can influence the ionization cross sections for the L_1 and L_2 subshells in the range 10–12 %. For the L_3 subshell, this effect is practically negligible.

IV. CONCLUSIONS

L-subshell ionization cross sections for selected heavy elements from Hf to Th were measured for ^{12}C and ^{14}N ion bombardment in the energy range 0.4–1.8 MeV/amu. The results for L_2-subshell ionization cross sections are systematically underestimated by the predictions of the ECPSSR and SCA theories up to a factor of 10 and 5, respectively. Observed discrepancies are expected to be related to the L-subshell coupling effects not accounted for in the theories discussed above. For higher energies ($\xi \approx 1$) the theories overestimate the data up to a factor of two, which is probably connected with the binding-polarization effects not fully accounted for in the calculations.

The ionization probabilities for the N_4 subshell were derived from the data. The results are compared with the predictions of the SCA theory and of the geometrical model. Possible changes of the atomic parameters used in the derivation of the L-subshell ionization cross sections due to multiple ionization effects are discussed.

ACKNOWLEDGMENTS

The authors are deeply indebted to the Tandem accelerator staff at the Institute of Physics of the Erlangen-Nürnberg University for their very kind collaboration during the measurements. This work was financially supported by the Federal Ministry for Research and Technology and by the Polish State Committee for Scientific Research.

[1] C. H. Rutlege and R. L. Watson, At. Data Nucl. Data Tables **12**, 197 (1973).
[2] T. L. Hardt and R. L. Watson, At. Data Nucl. Data Tables **17**, 107 (1976).
[3] R. K. Gardner and T. J. Gray, At. Data Nucl. Data Tables **21**, 515 (1978).
[4] H. Paul and J. Muhr, Phys. Rep. **135**, 47 (1986).
[5] C. Heitz, G. J. Costa, J. Cailleret, and G. Lagarde, Centre de Recherches Nucléaires, Université de Strasbourg, Report No. 82, 1982 (unpublished).
[6] R. S. Sokhi and D. Crumpton, At. Data Nucl. Data Tables **30**, 49 (1984).
[7] I. Orlič, C. H. Sow, and S. M. Tang, At. Data Nucl. Data Tables **56**, 159 (1994).
[8] R. Merzbacher and H. W. Lewis, Handb. Phys. **34**, 166 (1958).
[9] J. Bang and J. M. Hansteen, K. Dansk. Vidensk. Selsk. Mat. Fys. Medd. **31**, 13 (1959).
[10] W. Brandt, R. Laubert, and I. Sellin, Phys. Rev. **151**, 56 (1966).
[11] P. A. Amundsen, J. Phys. B **10**, 2177 (1977).
[12] M. Pauli and D. Trautmann, J. Phys. B **11**, 667 (1978).
[13] D. Jamnik and Č. Zupancič, K. Dansk. Vidensk. Selsk. Mat. Fys. Medd. **31**, 1 (1957).
[14] B. H. Choi, Phys. Rev. A **4**, 1002 (1971).
[15] P. A. Amundsen and L. Kocbach, J. Phys. B **8**, L122 (1975).
[16] P. A. Amundsen, J. Phys. B **10**, 1097 (1977).
[17] M. Pauli, F. Rösel, and D. Trautmann, J. Phys. B **11**, 2511 (1978).
[18] G. Basbas, W. Brandt, and R. Laubert, Phys. Rev. A **7**, 983 (1973).
[19] W. Brandt and G. Lapicki, Phys. Rev. A **10**, 474 (1974).
[20] W. Brandt and G. Lapicki, Phys. Rev. A **20**, 465 (1979).
[21] W. Brandt and G. Lapicki, Phys. Rev. A **23**, 1717 (1981).
[22] D. Trautmann and F. Rösel, Nucl. Instrum. Methods B **169**, 259 (1980).
[23] D. Trautmann and T. Kauer, Nucl. Instrum. Methods B **42**, 426 (1989).
[24] L. Sarkadi and T. Mukoyama, Nucl. Instrum. Methods B **61**, 167 (1991).
[25] J. Semaniak, J. Braziewicz, M. Pajek, A. P. Kobzev, and D. Trautmann, Nucl. Instrum. Methods B **75**, 63 (1992).
[26] L. Sarkadi and T. Mukoyama, J. Phys. B **14**, L255 (1981).
[27] L. Sarkadi and T. Mukoyama, Nucl. Instrum. Methods B **232**, 296 (1984).
[28] W. Jitschin, A. Kaschuba, R. Hippler, and H. O. Lutz, J. Phys. B **15**, 763 (1982).
[29] L. Sarkadi and T. Mukoyama, J. Phys. B **13**, 2255 (1980).
[30] N. B. Malhi and T. J. Gray, Phys. Rev. A **44**, 7199 (1991).
[31] R. Mehta, J. L. Duggan, F. D. McDaniell, M. R. McNeir, Y. C. Yu, D. K. Marble, and G. Lapicki, Nucl. Instrum. Methods B **79**, 175 (1992).
[32] J. Pálinkás, L. Sarkadi, B. Schlenk, I. Török, Gy. Kálmán, C. Bauer, K. Brankoff, D. Grambole, C. Heiser, W. Rudolph, and H. J. Thomas, J. Phys. B **17**, 131 (1983).
[33] C. Bauer, H. Richter, P. Gippner, R. Mann, W. Rudolph, B. Eckhard, and K. O. Groeneveld, Z. Phys. A **303**, 13 (1981).
[34] M. Pajek, A. P. Kobzev, R. Sandrik, R. A. Ilkhamov, and S. H. Khusmurodov, Nucl. Instrum. Methods B **42**, 346 (1989).
[35] M. C. Lépy and J. Plagnard (unpublished).
[36] V. B. Zlokazov, Comput. Phys. Commun. **28**, 27 (1982).
[37] E. Huttel, W. Arnold, H. Baumgart, and G. Clausnitzer, Nucl. Instrum. Methods B **12**, 193 (1985).
[38] M. Pajek, A. P. Kobzev, R. Sandrik, A. V. Skrypnik, R. A. Ilkhamov, S. H. Khusmurodov, and G. Lapicki, Phys. Rev. A **42**, 261 (1990).
[39] J. F. Ziegler, J. P. Biersack, and U. Littmark, *The Stopping Range of Ions in Solids* (Pergamon, New York, 1985), Vol. 1.
[40] J. H. Scofield, At. Data Nucl. Data Tables **14**, 121 (1974).
[41] M. H. Chen, B. Crasemann, and H. Mark, Phys. Rev. A **24**, 177 (1981).
[42] A. Berinde, C. Ciortea, A. Enulescu, D. Fluerasu, G. Hock, I. Piticu, L. Sarkadi, B. Sulik, and V. Zoran, J. Phys. B **20**, L481 (1987).
[43] A. Berinde, C. Ciortea, A. Enulescu, D. Fluerasu, I. Piticu, and V. Zoran, Nucl. Instrum. Methods B **232**, 283 (1984).
[44] G. Lapicki and F. D. McDaniel, Phys. Rev. A **22**, 1896 (1980).
[45] J. C. Slater, Phys. Rev. **36**, 57 (1930).
[46] M. Vigilante, P. Cuzzocrea, N. De Cesare, F. Murollo, E. Perillo, and G. Spadaccini, Nucl. Instrum. Methods B **51**, 232 (1990).
[47] M. Pajek, A. P. Kobzev, D. Trautmann, and T. Kauer, Nucl. Instrum. Methods B **52**, 109 (1990).
[48] L. Sarkadi, J. Phys. B **19**, L755 (1986).
[49] L. Sarkadi, J. Phys. B **19**, 2519 (1986).
[50] G. Mehler, J. Reinhardt, B. Müller, W. Greiner, and G. Soff, Z. Phys. D **5**, 143 (1977).
[51] P. A. Amundsen and D. H. Jakubassa-Amundsen, J. Phys. B **21**, L99 (1988).
[52] M. O. Krause, J. Phys. Chem. Ref. Data **8**, 307 (1979).
[53] D. Bhattacharaya, G. Kuri, D. P. Mahapatra, M. B. Chatterjee, and P. Sen, Z. Phys. D **28**, 123 (1993).
[54] B. Sulik, I. Kádár, S. Rich, D. Varga, I. Végh, G. Hock, and D. Berényi, Nucl. Instrum. Methods B **28**, 509 (1981).
[55] J. H. McGuire and P. Richard, Phys. Rev. A **8**, 1374 (1973).
[56] W. Jitschin, R. Hippler, R. Shanker, R. Kleinpoppen, R. Schuch, and H. O. Lutz, J. Phys. B **16**, 1417 (1983).
[57] F. M. Parente, H. Chen, B. Crasemann, and H. Mark, At. Data Nucl. Data Tables **26**, 383 (1981).
[58] G. Lapicki, R. Mehta, J. L. Duggan, P. M. Kocur, J. L. Price, and F. D. McDaniel, Phys. Rev. A **34**, 3813 (1986).